

Solvothermal synthesis and characterization of size-controlled monodisperse Fe_3O_4 nanoparticles

Guanhua Gao · Rongrong Shi · Wenqing Qin ·
Youguo Shi · Guofu Xu · Guanzhou Qiu · Xiaohe Liu

Received: 26 September 2009 / Accepted: 3 March 2010 / Published online: 2 April 2010
© Springer Science+Business Media, LLC 2010

Abstract Monodisperse Fe_3O_4 nanoparticles with narrow size distribution could be successfully synthesized in large quantities by a facile solvothermal synthetic method in the presence of oleic acid and oleylamine. Well-defined assembly of uniform nanoparticles with average sizes of 8 nm can be obtained without a further size-selection process. The sizes of final products could be readily tuned from 5 to 12 nm by adjusting the experimental parameters such as reaction time, temperature, and surfactants. The phase structures, morphologies, and magnetic properties of the as-prepared products were investigated in detail by X-ray diffraction, transmission electron microscopy, selected area electron diffraction, high-resolution transmission electron microscopy, and magnetometry with a superconducting quantum interference device. The magnetic study reveals that the as-synthesized nanoparticles are ferromagnetic at 2 K while they are superparamagnetic at 300 K.

Introduction

Magnetic materials have for many years been attracting great attention and interest due to their technological and fundamental scientific importance and their wide use in several practical applications. Monodisperse magnetic nanoparticles often exhibit very interesting electronic, optical, and magnetic properties, which cannot be achieved by their bulk counterparts. Over the past few decades, much attention has been focused on the development of monodisperse magnetite nanoparticles having uniform sizes and narrow-size distributions [1–7]. Especially, the synthesis of magnetic nanoparticles with controlled sizes and shapes has been intensively pursued because of their size- and shape-dependent functional properties in electricity, magnetism, and so on [8–14]. It is well known that the monodisperse magnetic particles can be assembled into highly ordered 2D or 3D structure, and may exhibit fascinating physical and chemical properties conducive for the potential applications in many fields such as magnetic recording media, ferrofluids, and catalysts [15–17]. Properly coated or surface-modified magnetic nanoparticles have been successfully used in biomedical fields, e.g., biological labeling, detection and separation, target-drug delivery and magnetic resonance imaging, etc. [18–23]. So far, various chemical methods have been applied to fabricate magnetic nanoparticles, such as sol–gel technique [24, 25], co-precipitation process [26], reverse micelle method [27], and hydrothermal/solvothermal treatment [28–36]. However, magnetic nanoparticles usually tend to aggregate due to their intrinsic agglomerating properties. Therefore, the aggregation of magnetic nanoparticles presents a puzzle that needs to be resolved by materials scientists and chemists. Recently, a significant breakthrough was achieved in the synthesis of monodisperse magnetic

G. Gao · R. Shi · W. Qin (✉) · G. Qiu · X. Liu (✉)
Department of Inorganic Materials, Central South University,
Changsha 410083, Hunan, People's Republic of China
e-mail: qwq@mail.csu.edu.cn

X. Liu
e-mail: liuxh@mail.csu.edu.cn

Y. Shi
International Center for Materials Nanoarchitectonics (MANA),
National Institute for Materials Science, Namiki 1-1, Tsukuba,
Ibaraki 305-0044, Japan

G. Xu
School of Materials Science and Engineering,
Central South University, Changsha 410083, Hunan,
People's Republic of China

nano particles using thermal decomposition method [37–39]. Although this synthetic route is available for production of monodisperse nanocrystals, it usually involves complicated process and requires expensive apparatus.

In this study, we have developed a facile solvothermal method to fabricate monodisperse magnetite (Fe_3O_4) nanoparticles using iron acetylacetone (Fe(acac)₃) as precursor, oleic acid, oleylamine, and Tri-*n*-octylphosphine oxide (TOPO) as surfactants, and diethylene glycol as both reductant and solvent. The sizes of final products could be readily tuned from 5 to 12 nm through adjustment of the experimental parameters such as reaction time, temperature, and surfactants. The analysis of their magnetic properties reveals that the as-synthesized nanoparticles are ferromagnetic at 2 K while they are superparamagnetic at 300 K. Organic-phase synthetic methods have been widely used to synthesize nanoparticles because of their many advantages, such as the high crystallinity and good monodispersity of the synthesized nanoparticles, and their highly dispersible characteristic in organic solvents [4]. Moreover, this synthetic strategy presented in this article may prove to be a promising potential suitable for applications in the future and provide an effective route for the synthesis of other monodisperse nanostructural and functional materials under appropriate conditions.

Experimental section

The chemicals used in this study, such as iron acetylacetone (Fe(acac)₃), diethylene glycol, *n*-hexane, and anhydrous ethanol were of analytical grade and put into use as starting materials without further purification. Tri-*n*-octylphosphine oxide (TOPO, 99%), oleic acid, and oleylamine were purchased from ACROS.

Synthesis

In a typical procedure for fabrication of 8-nm Fe_3O_4 nanoparticles, 0.3532 g (1 mmol) Fe(acac)₃ and 0.1935 g (0.5 mmol) TOPO were dissolved in 20 mL diethylene glycol solution containing 1.2 mL (4 mmol) oleic acid and 3.3 mL (10 mmol) oleylamine at room temperature; the mixture was stirred for several minutes to form a homogeneous solution, and then was put into a Teflon-lined stainless steel autoclave with a capacity of 40 mL. Before sealing the autoclave, argon was bubbled into the solution to remove the air. The autoclave was first maintained at 200 °C for 30 min and then heated further to raise the temperature to be maintained at 260 °C for 2 h. After the completion of the reaction, the autoclave was cooled to room temperature in natural ambience. The product was washed with hexane and anhydrous ethanol several times,

and finally dried in vacuum at 60 °C for 4 h. The amount of TOPO, ratio of oleic acid to oleylamine, and the reaction temperature and time were also described.

Characterization

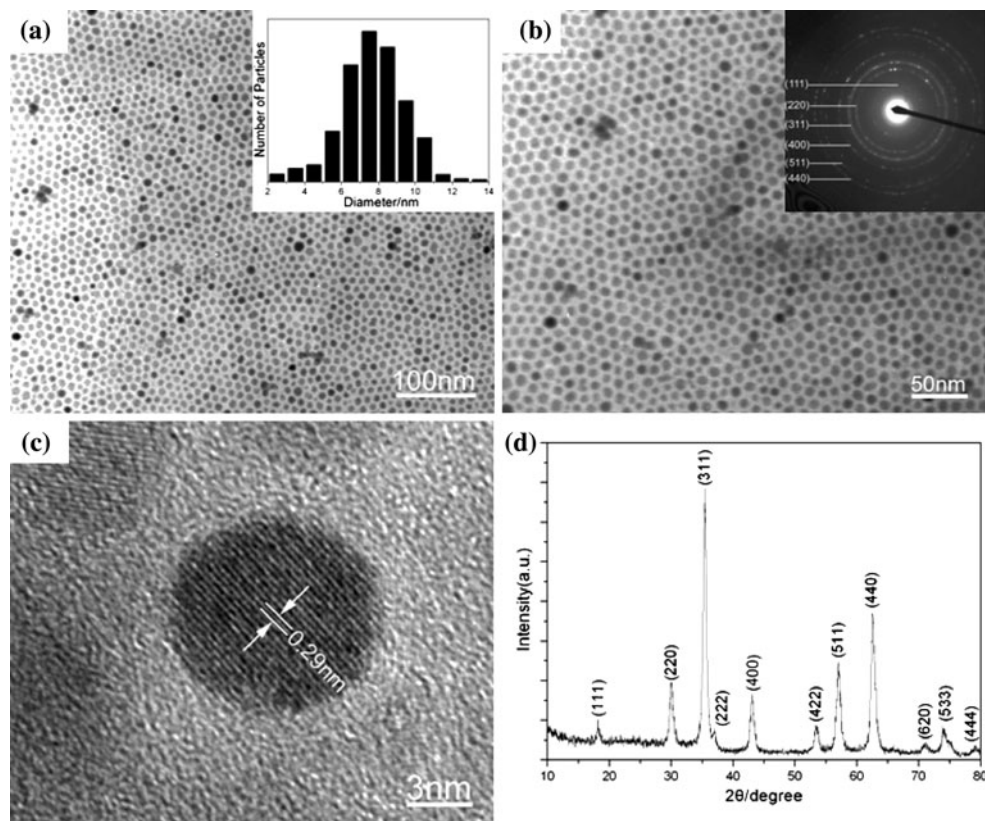
The samples obtained were characterized on a D/max2550 VB + X-ray powder diffraction (XRD) with Cu K α radiation ($\lambda = 1.54178 \text{ \AA}$). The operating voltage and current were kept at 40 kV and 40 mA, respectively. The size and morphology of the as-prepared products were determined at 160 kV by a JEM-200CX transmission electron microscope (TEM) and a JEOL JEM-2010F high-resolution transmission electron microscope (HRTEM). The magnetic properties were measured with Quantum Design superconducting quantum interference device (SQUID).

Results and discussion

Transmission electron microscope (TEM) was employed to characterize the morphology, size, and size distribution of the as-prepared products. The low- and high-magnification TEM images of Fe_3O_4 nanoparticles obtained at 260 °C for 2 h using 0.5 mmol TOPO with molar ratio of oleic acid to oleylamine as 4:10 are shown in Fig. 1a and b. It can be observed that monodisperse Fe_3O_4 nanoparticles with good uniformity in large quantities were successfully achieved under current experimental conditions. As shown in Fig. 1a and b, most of these products display spherical shapes with smooth surface and the mean diameter is about 8 nm. The particle size histogram inserted in Fig. 1a shows a narrow size distribution of the product. The corresponding selected area electron diffraction (SAED) pattern inserted in Fig. 1b reveals the satisfactory crystallinity of the sample, which can be well indexed to the spinel structure of pure Fe_3O_4 . High-resolution transmission electron microscopy provides further insight into the nanostructure of the as-prepared Fe_3O_4 nanoparticles. Figure 1c shows the HRTEM image of an individual Fe_3O_4 nanoparticle with a diameter of about 8 nm. Adjacent fringe spacing was measured to be 0.297 nm, which is consistent with the interplanar spacing of (220) planes of face-centered cubic. X-ray diffraction (XRD) pattern is displayed in Fig. 1d. All diffraction peaks can be readily indexed to the pure face-centered cubic phase [space group: $Fd\bar{3}m$ (227)] of Fe_3O_4 with cell constants $a = 8.393 \text{ \AA}$, which agrees well with the reported diffraction pattern (data from JCPDS file No. 85-1436). No impurity peak was observed, indicating that the pure Fe_3O_4 with spinel structure was successfully synthesized under the experimental conditions of this study.

In order to arrive at a better understanding of the growth process of Fe_3O_4 nanoparticles, a series of experiments

Fig. 1 **a** Low- and **b** higher-magnification TEM images of the as-prepared Fe_3O_4 nanoparticles prepared at 260 °C for 2 h using 0.5 mmol TOPO with molar ratio of oleic acid to oleylamine as 4:10. The inset of **a** shows the corresponding particle size distribution histogram. The inset of **b** shows the selected area electron diffraction (SAED) pattern of the Fe_3O_4 nanoparticles acquired from sample A. **c** HRTEM image of an individual Fe_3O_4 nanoparticle. **d** XRD pattern of the as-prepared Fe_3O_4 nanoparticles

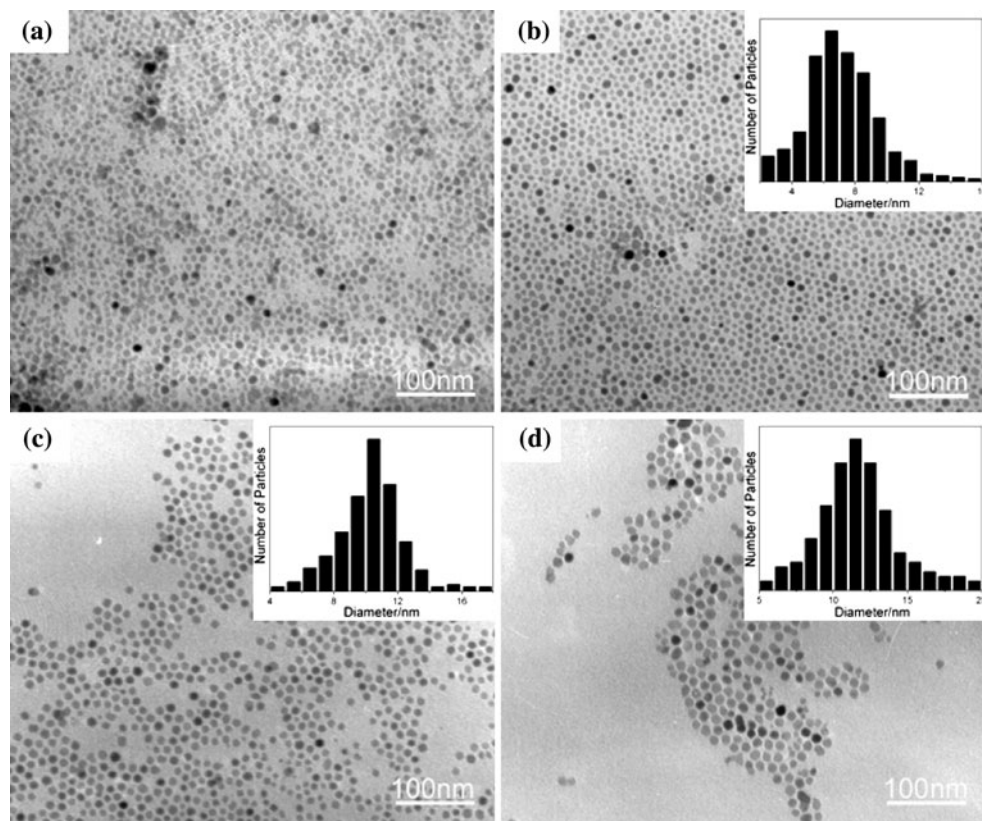


under different reaction conditions were carried out. It is found that the morphologies and sizes of final products strongly depended on reaction conditions such as reaction temperature, solvothermal time, and surfactants. Figure 2 displays TEM images of the as-prepared Fe_3O_4 nanoparticles obtained with different reaction temperatures and times. The as-prepared products obtained at 220 °C for 2 h display irregular shapes and wide particle size distribution (Fig. 2a). When the temperature was increased to 240 °C for 2 h, the products show roughly spherical-shaped particles (Fig. 2b). The corresponding size distribution histogram inserted in Fig. 2b shows that the product is about 6.5 nm with good monodispersity, and its size distribution is concentrated in the range of 5–8 nm. The product obtained and maintained at the temperature of 260 °C for 2 h is shown in Fig. 1a, wherein one can clearly see that the size and morphology of product show the trend of a more uniform and regular structure. We found that the elevated temperature process produces more uniform samples with relatively round particles. In the current synthesis, as the optimal reaction temperature (260 °C) is higher than the boiling point of diethylene glycol (245 °C), the production of the more uniformly sized Fe_3O_4 particles seems to indicate that high reaction temperature will be necessary and favorable for the formation of homogeneous magnetic nanoparticles. This phenomenon may be attributed to the fact that the high temperature of 260 °C allows

a sufficient reaction rate, while the low temperature decreases the reaction rate and the diffusion of active species which broadens the size distribution and induces disproportionation and aggregation. The impact of reaction time on the formation of size-controlled Fe_3O_4 nanoparticles was significant in the synthesis. TEM images of the nanoparticles obtained at 260 °C for different reaction times are shown in Fig. 2c and d. The size of Fe_3O_4 nanoparticles gradually increased with the prolongation of the reaction time. After prolonging the reaction time to 6 h, monodisperse Fe_3O_4 nanoparticles with narrow size distribution were obtained, with the mean diameter increasing to approximately 10.5 nm (Fig. 2c). On further prolongation of the reaction time to 12 h, the mean size of Fe_3O_4 nanoparticles was measured to be 12 nm (Fig. 2d). These results indicate that the sizes of Fe_3O_4 nanoparticles linearly increase with increasing reaction temperature and time.

The influence of surfactant TOPO on the morphology and size distribution of the as-synthesized Fe_3O_4 nanoparticles was also investigated. We found that the amount of TOPO plays a crucial role in the morphology of Fe_3O_4 nanoparticles under solvothermal conditions. Figure 3 shows the typical TEM images of the as-prepared Fe_3O_4 nanoparticles obtained by varying the amounts of TOPO while keeping the other parameters constant. The product obtained without TOPO is shown in Fig. 3a, which exhibits

Fig. 2 The TEM images of Fe_3O_4 nanoparticles prepared at different reaction conditions. **a** 220 °C, 2 h **b** 240 °C, 2 h **c** 260 °C, 6 h **d** 260 °C, 12 h. The insets are the corresponding particle size distribution histograms

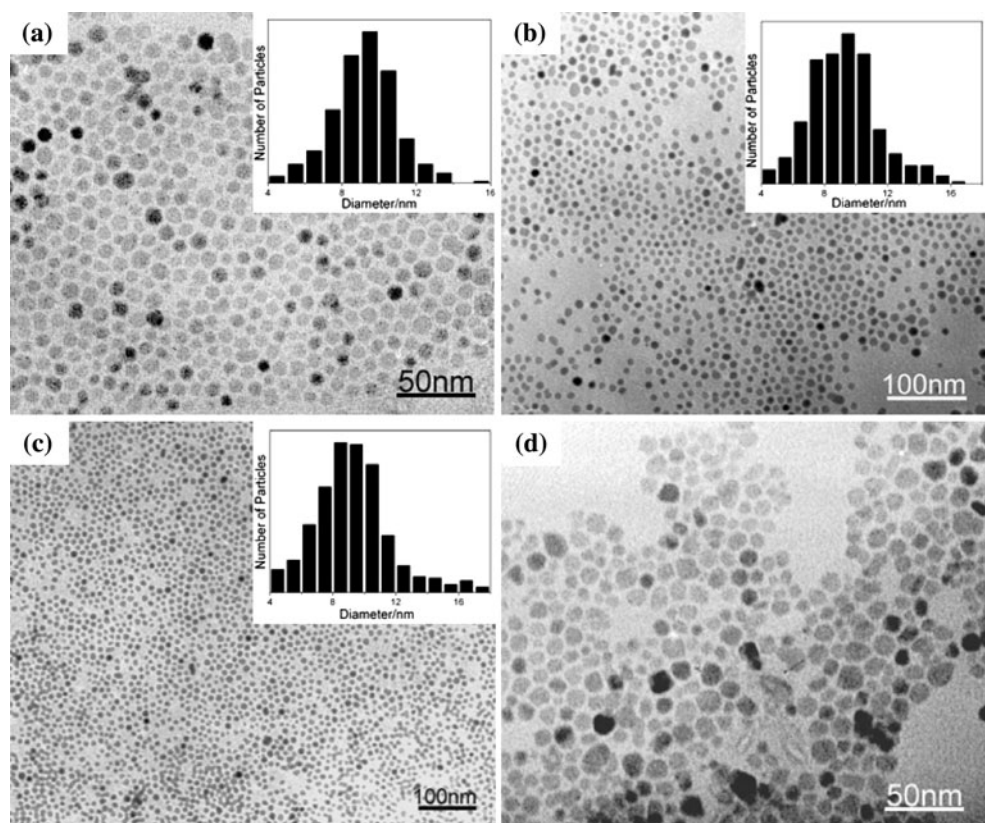


good uniformity in both particle size and morphology. From the TEM image of Fig. 3b, we can see that the product with 0.1 mmol TOPO displays a wide size distribution. On further increasing the amount of TOPO from 0.1 to 0.3 mmol, the uniformity of particle sizes improved indistinctively, and the particle size distribution inserted in Fig. 3c was similar with that inserted in Fig. 3b. The amount of TOPO was further increased to 0.5 mmol, the product presents a uniformly ordered 2D structure in closely packed manner, implying that the uniform monodisperse Fe_3O_4 nanoparticles were obtained (Fig. 1a). However, the uniformity of the product deteriorated and irregular shaped particles resulted, when the amount of TOPO was enhanced to 1 mmol (Fig. 3d). These results reveal that TOPO is an effective surfactant in the solvothermal process adopted in this study; however, its excessive amount is disadvantageous for the uniformity of monodisperse Fe_3O_4 nanoparticles. It is reported that TOPO can be applied as a stabilizing surfactant in the synthetic process of monodisperse Fe_3O_4 nanoparticles [40]. However, the detailed nature of surfactant TOPO serving as a capping agent or steric stabilizer has rarely been reported in the literature. We believe that in this experimental study, Fe in $\text{Fe}(\text{acac})_3$ has electronic empty orbit, whereas O doubly bonded with P has redundant electron in TOPO monomer. Under heat treatment, $\text{Fe}(\text{acac})_3$ and TOPO synthesize a chelating ligand, then the

resulting small Fe_3O_4 crystals nucleate and grow. The smaller nanoparticles dissolved and deposited on the bigger nanoparticles. These results are consistent with the Ostwald's ripening process [6] wherein large particles grow at the expense of smaller ones.

In order to study the effect of oleic acid and oleylamine on the products further, we designed two experiments for comparison, one with the presence of only the oleic acid and the other with the presence of only the oleylamine. The corresponding results are shown in Fig. 4a and b, respectively. The product without oleic acid displays bad dispersibility in the field of view (Fig. 4a). With the use of oleic acid alone, the TEM image of the product as shown in Fig. 4b, exhibits Fe_3O_4 nanoparticles with irregular shapes. Inspired by the results mentioned above, the molar ratio of oleic acid to oleylamine was changed in the experiments. Figure 4c and d show the TEM images of Fe_3O_4 nanoparticles using different amounts of oleylamine while keeping the amount of oleic acid fixed. The as-prepared Fe_3O_4 nanoparticles with the molar ratio of oleic acid to oleylamine as 4:4 were irregular and aggregated slightly (Fig. 4c). Increasing the amount of oleylamine to 16 mmol, one can see that some particles with similar diameters congregated to form short chains, and the boundaries of those particles were blurry (Fig. 4d). The inset of Fig. 4d shows the mean diameter is about 5.3 nm, which is smaller than that of Fe_3O_4 nanoparticles prepared with a

Fig. 3 The TEM images of Fe_3O_4 nanoparticles obtained at 260 °C for 2 h with molar ratio of oleic acid to oleylamine 4:10 by using different amount of TOPO: **a** without TOPO **b** 0.1 mmol **c** 0.3 mmol **d** 1.0 mmol. The insets are the corresponding particle size distribution histograms



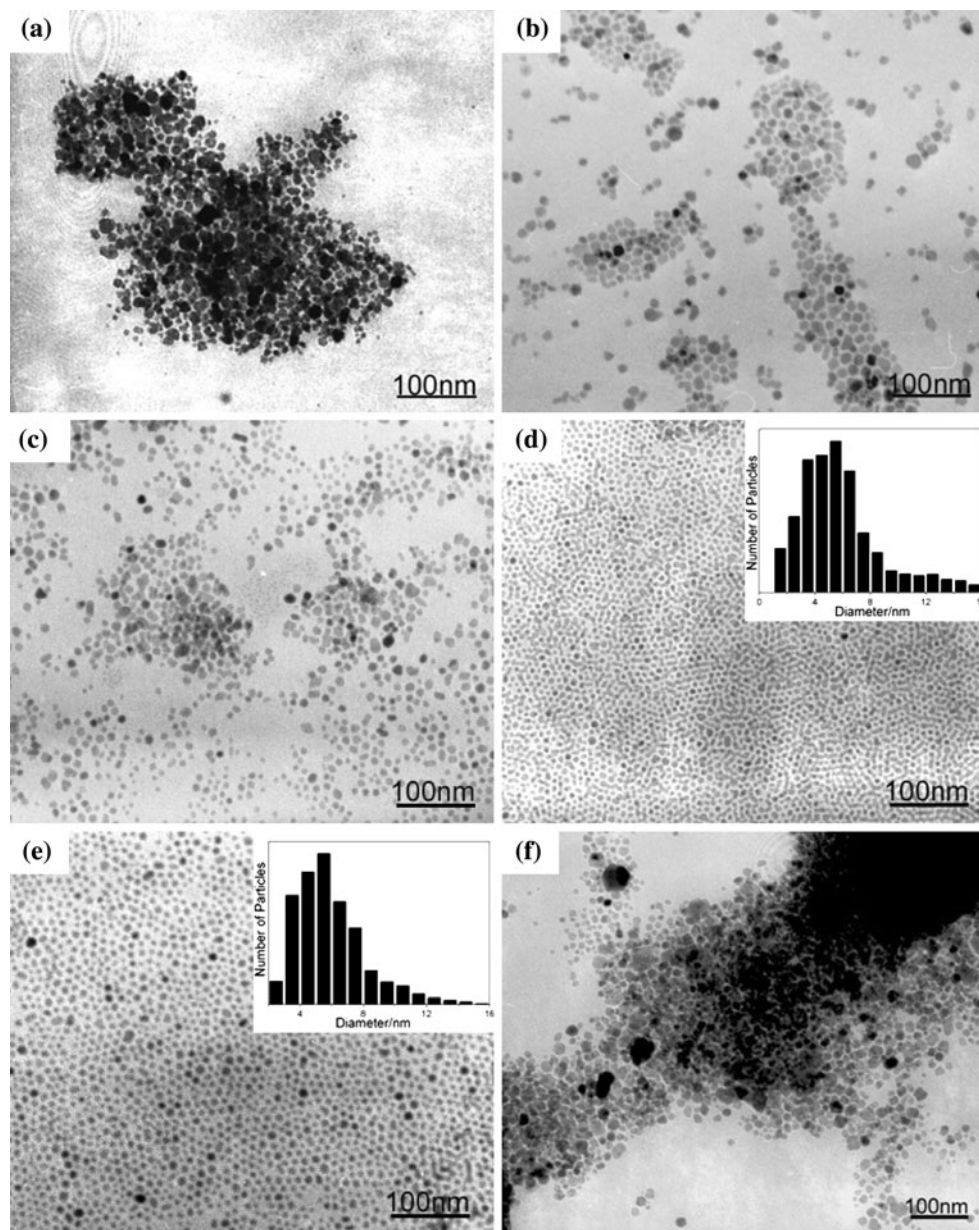
4:10 molar ratio. On the other hand, on reducing the amount of oleic acid from 4 mmol to 1 mmol, we could get a product with good monodispersity, but the size distribution was relatively broader (Fig. 4e). Furthermore, it was found that the as-synthesized nanoparticles in Fig. 4f aggregated intensively when the molar ratio was set as 10:10. This is probably caused by the excessive amount of oleic acid, which increases the viscosity of the system and prevents the diffusion of reactive species. Oleic acid, as one of the commonly used capping agents in the synthesis of monodisperse nanoparticles, shows a strong binding to the surface sites and stabilizes the particle growth [5, 41]. In this study, the surface iron atoms of the nanoparticles were in coordination with the carboxylic acid groups of oleic acid ligands, forming a steric-stabilizing layer that prevented nanoparticles' aggregation and facilitated the formation of monodisperse samples. In addition, oleylamine is much more important for obtaining the smaller nanoparticles. On comparison of the Fe_3O_4 nanoparticles while synthesizing with different amounts of oleylamine, we observe that the experimental results mentioned above have proven this point. These results of surface modification in the organic phase indicate that the carboxylic and amino groups are capable of stabilizing the surface of magnetite to produce smaller nanoparticles [28].

The exact mechanism leading to Fe_3O_4 in the reaction under this study is not yet clear. However, for

homogeneous synthesis, the key to synthesizing monodisperse nanoparticles is to precisely control the nucleation process and the growth process. Decomposition of precursors with cationic metal centers leads directly to the corresponding metal oxides [17]. Thus, we speculate that when the temperature is increased, the $\text{Fe}(\text{acac})_3$, the precursor, begins to decompose. The decomposition temperature of $\text{Fe}(\text{acac})_3$ is about 190 °C. As soon as the temperature reached ~190 °C, $\text{Fe}(\text{acac})_3$ could be decomposed to form Fe_3O_4 nuclei. Keeping the mixture at 200 °C for 30 min before it was heated to 260 °C ensured the homogeneous nucleation, which facilitated the production of monodisperse nanoparticles, since the processes of the nucleation of Fe_3O_4 and the growth of the nuclei under current conditions are not fast, which agreed with the previous study in the literature [2]. Diffusion of growth species through the highly viscous diethylene glycol–oleic acid–oleylamine system to many growing crystallites would be slow, thus limiting the Fe_3O_4 crystallite's growth and preventing them from aggregation. These conditions are favorable for the formation of monodisperse particles.

The magnetic properties of monodisperse Fe_3O_4 nanoparticles prepared at 260 °C for 2 h using 0.5 mmol TOPO, 4 mmol oleic acid, and 10 mmol oleylamine were investigated through Quantum Design SQUID. Representative hysteresis loops of the as-prepared Fe_3O_4 measured at 2 and 300 K are shown in Fig. 5. The magnetic study reveals

Fig. 4 The TEM images of Fe_3O_4 nanoparticles obtained at 260 °C for 2 h with 0.5 mmol TOPO by using different molar ratio of oleic acid to oleylamine: **a** 10 mmol oleylamine without oleic acid **b** 4 mmol oleic acid without oleylamine **c** 4:4 **d** 4:16 **e** 1:10 **f** 10:10. The insets are the corresponding particle size distribution histograms



that the as-synthesized nanoparticles are ferromagnetic at 2 K while they are superparamagnetic at 300 K. The saturation magnetization (M_s) and coercivity (H_c) of the product are 75.5 emu/g and 550 Oe at 2 K, respectively. The saturation magnetization is 68.1 emu/g at 300 K. This result shows the lower magnetization characteristics of final products in comparison to that of the commercially available Fe_3O_4 power ($M_s = 83$ emu/g). Nanoparticles prepared by various methods usually possess different surface coordinations, which exert a great influence on the magnetic properties of the nanoparticles [17, 27]. In our synthesis, Fe_3O_4 nanoparticles were synthesized in organic phase in the presence of oleic acid and oleylamine, and the surface of as-prepared nanoparticles may be covered by a

layer of organic molecules. Therefore, the existence of surfactants on the surface of Fe_3O_4 nanoparticles most likely contributes to the decrease of the saturation magnetization.

Conclusions

In summary, we have successfully synthesized monodisperse Fe_3O_4 nanoparticles via a convenient solvothermal synthetic route under mild conditions. The sizes of final products could be effectively tuned from 5 to 12 nm by altering several factors including reaction time, temperature, and surfactants. The analysis of magnetic

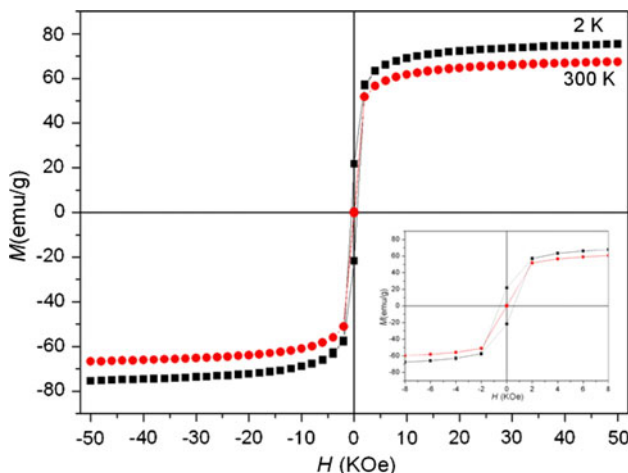


Fig. 5 Hysteresis loops of Fe_3O_4 nanoparticles obtained at 260 °C for 2 h using 0.5 mmol TOPO with molar ratio of oleic acid to oleylamine as 4:10 measured at 2 and 300 K. The *inset* is the enlarged hysteresis loops

characteristics reveals that the as-synthesized nanoparticles are ferromagnetic at 2 K while they are superparamagnetic at 300 K. It is expected that the monodisperse Fe_3O_4 nanoparticles exhibit many important applications in, e.g., magnetic recording media, ferrofluids, catalysis, biomedical fields, etc. It is worthy to note that this relatively safe and convenient synthetic strategy may be applied to synthesize other monodisperse nanostructural materials under appropriate conditions, and provide good prospects for use in future large-scale applications owing to its advantages, such as high yield, simple design of the apparatus, and mild conditions.

Acknowledgements Financial support of this work by National Natural Science Foundation of China (No. 50504017) and Hunan Provincial Key Science and Technology Project of China (No. 2007FJ3008) is gratefully acknowledged.

References

1. Fried T, Shemer G, Markovich G (2001) *Adv Mater* 13:1158
2. Sun SH, Zeng H, Robinson DB, Raoux S, Rice PM, Wang SX, Li GX (2004) *J Am Chem Soc* 126:273
3. Yang TZ, Shen CM, Yang HT, Xiao CW, Xu ZC, Chen ST, Shi DX, Gao HJ (2006) *Surf Interface Anal* 38:1063
4. Park J, Joo J, Kwon SG, Jang Y, Hyeon T (2007) *Angew Chem Int Ed* 46:4630
5. Cushing BL, Kolesnichenko VL, O'Connor CJ (2004) *Chem Rev* 104:3893
6. Jeong U, Teng X, Wang Y, Yang H, Xia Y (2007) *Adv Mater* 19:33
7. Shi RR, Liu XH, Gao GH, Yi R, Qiu GZ (2009) *J Alloys Compd* 485:548
8. Yang HT, Ogawa T, Hasegawa D, Takahashi M (2008) *J Appl Phys* 103:07D526
9. Yang DP, Gao F, Cui DX, Yang M (2009) *Curr Nanosci* 5:485
10. Kim D, Lee N, Park M, Kim BH, An K, Hyon T (2009) *J Am Chem Soc* 131:454
11. Zhang DE, Wu W, Li SZ, Zhang XB, Han GQ, Ying AL, Gong JY, Tong ZW (2010) *J Mater Sci* 45:34. doi:[10.1007/s10853-009-3866-0](https://doi.org/10.1007/s10853-009-3866-0)
12. Wang LL, Gao L (2009) *J Phys Chem C* 113:15914
13. Bi HY, Wang XQ, Li HB, Xi BJ, Zhu YC, Qian YT (2009) *Solid State Commun* 149:2115
14. Bai W, Meng XJ, Zhu X, Jing CB, Gao C, Chu JH (2009) *Physica E* 42:141
15. Kim DK, Mikhaylova M, Wang FH, Kehr J, Bjelke B, Zhang Y, Tsakalatos T, Muhammed M (2003) *Chem Mater* 15:4343
16. Jiang JS, Gan ZF, Yang Y, Du B, Qian M, Zhang P (2009) *J Nanopart Res* 11:1321
17. Lu A-H, Salabas EL, Schüth F (2007) *Angew Chem Int Ed* 46:1222
18. Liu SH, Xing RM, Lu F, Rana RK, Zhu J-J (2009) *J Phys Chem C* 113:21042
19. Grancharov SG, Zeng H, Sun SH, Wang SX, O'Brien S, Murray CB, Kirtley JR, Held GA (2005) *J Phys Chem B* 109:13030
20. Yang HH, Zhang SQ, Chen XL, Zhuang ZX, Xu JG, Wang XR (2004) *Anal Chem* 76:1316
21. Giri S, Trewyn BG, Stellmacher MP, Lin VS-Y (2005) *Angew Chem Int Ed* 44:5038
22. Zhang JL, Srivastava RS, Misra RDK (2007) *Langmuir* 23:6342
23. Brähler M, Georgieva R, Buske N, Müller A, Müller S, Pinkernelle J, Teichgräber U, Voigt A, Bäumler H (2006) *Nano Lett* 6:2505
24. Wu W, Xiao XH, Zhang SF, Li H, Zhou XD, Jiang CZ (2009) *Nanoscale Res Lett* 4:926
25. Eken AE, Ozenbas M (2009) *J Sol-Gel Sci Technol* 50:321
26. Li Z, Tan B, Allix M, Cooper AI, Rosseinsky MJ (2008) *Small* 4:231
27. Vestal CR, Zhang ZJ (2003) *J Am Chem Soc* 125:9828
28. Takami S, Sato T, Mousavand T, Ohara S, Umetsu M, Adschiri T (2007) *Mater Lett* 61:4769
29. Dong Q, Kumada N, Yonesaki Y, Takei T, Kinomura N (2009) *J Ceram Soc Jpn* 117:881
30. Qu X-F, Zhou G-T, Yao Q-Z, Fu S-Q (2010) *J Phys Chem C* 114:284
31. Wang Q, Wu AB, Yu LX, Liu ZL, Xu W, Yang H (2009) *J Phys Chem C* 113:19875
32. Zhao S, Asuha S (2010) *Powder Technol* 197:295
33. Si SF, Li CH, Wang X, Yu DP, Peng Q, Li YD (2005) *Cryst Growth Des* 5:391
34. Wang J, Yao M, Xu GJ, Cui P, Zhao JT (2009) *Mater Chem Phys* 113:6
35. Qi HP, Chen QW, Wang MS, Wen MH, Xiong J (2009) *J Phys Chem C* 113:17301
36. Lu J, Jiao XL, Chen DR, Li W (2009) *J Phys Chem C* 113:4012
37. Adireddy S, Lin C, Palshin V, Dong Y, Cole R, Caruntu G (2009) *J Phys Chem C* 113:20800
38. Cheng C-J, Lin C-C, Chiang R-K, Lin C-R, Lyubutin IS, Alkaev EA, Lai H-Y (2008) *Cryst Growth Des* 8:877
39. Moriya M, Ito M, Sakamoto W, Yogo T (2009) *Cryst Growth Des* 9:1889
40. Hyeon T (2003) *Chem Commun* 8:927
41. Willis AL, Turro NJ, O'Brien S (2005) *Chem Mater* 17:5970